High Pitch Helical CT Reconstruction

John W. Hayes, Juan Montoya, Adam Budde, Chengzhu Zhang, Yinsheng Li, Ke Li, Jiang Hsieh, and Guang-Hong Chen

***Abstract*— To avoid severe limited-view artifacts in reconstructed CT images, current multi-row detector CT (MDCT) scanners with a single x-ray source-detector assembly need to limit table translation speeds such that the pitch p (viz., normalized table translation distance per gantry rotation) is lower than 1.5. When $p > 1.5$, it remains an open question whether one can reconstruct clinically useful helical CT images without severe artifacts. In this work, we show that a synergistic use of advanced techniques in conventional helical filtered backprojection, compressed sensing, and more recent deep learning methods can be properly integrated to enable accurate reconstruction up to $p = 4$ without significant artifacts for single source MDCT scans.**

***Index Terms*— X-ray CT, MDCT, deep learning, compressed sensing, image reconstruction.**

I. Introduction

MULTI-ROW detector CT (MDCT) scanners are primary workhorses in hospitals and clinics around the world. They allow patients to be scanned continuously to increase the scan throughput which is often defined as the scan volume per unit time. With the increase of detector rows from single slice scanners dating back to the early 1990s to the current popular 64-slice scanners and high-end 256-slice scanners, the anatomical coverage along the superior/inferior (SI) direction, viz., z-direction, can be as wide as 16 cm per scan rotation [1]. With more detector rows to increase coverage, the cost of scanners also escalates significantly. As a good balance between the cost and clinical scan throughput, it is the MDCT scanners with 64-slice or fewer that are predominantly used in current clinical applications. There are two modes of data acquisition in MDCT: axial scanning where the patient remains stationary or helical CT (also called spiral CT) where the patient is translated along the SI direction while the detector-source assembly rotates around the patient. Helical CT was introduced to the clinic in the early 1990s [2]–[4], revolutionizing the modality and making it easier and faster to scan larger patient volumes, enabling the scan of an entire organ in a single breath-hold. Presently, helical scanning is used for the vast majority of scans in the clinic and is used to scan all parts of the body including the chest [5], heart [6], abdomen and pelvis [7], head [8], and extremities [9].

Different from the ordinary circular scans where the view angles in a CT acquisition can be considered to be distributed on a circular trajectory, the view angles in helical CT scan mode are effectively distributed on a three-dimensional curve, i.e., a helix. Given a certain number of view angles, the sampling density of view angles depends on the geometrical coverage along the z-direction. The longer the z-coverage, the lower the view angle sampling density. The coverage along the z-direction per helical turn is defined as helical pitch in mathematical literature. However in helical CT, due to the use of multi-row detectors in data acquisitions, the anatomical coverage along the SI direction per gantry rotation depends on the number of detector rows in MDCT. To eliminate the potential confusion, helical pitch in the CT community is defined as the linear distance travelled by the CT couch per gantry rotation normalized by the detector collimation at isocenter [10]. Therefore, helical pitch in the CT community is defined as a dimensionless ratio while the helical pitch in other scientific contexts may mean the extended height of a helix turn with a physical unit of length.

For current single source MDCT scanners, the helical pitch, p, is often restricted to below 1.5. This restriction is due to the presence of image artifacts for pitches larger than 1.5 if current state-of-the-art reconstruction algorithms are used to reconstruct images. As it will be elaborated more carefully in Section II-A, the angular range illuminating each image voxel decreases as pitch increases. When $p > 1.5$, the view angle ranges for the image pixels in a reconstruction plane at $z = z_0$ fall well below the Tuy data sufficiency condition [11]. Therefore, there are two intrinsic scientific challenges in high pitch helical CT reconstruction problems: 1) the angular sample interval is large—as that in view angle undersampled reconstruction problems in circular scans—and 2) the view angle range is also truncated—as that in limited view angle reconstruction problems. As a result of these scientific challenges, high pitch helical reconstruction suffers from two main types of image artifacts: limited view artifacts and artifacts caused by the data inconsistency along the z-direction.

Despite the challenges in image reconstruction, high pitch helical scans are highly desirable in clinical practices due to the following important potential benefits: 1) As radiation

Manuscript received April 13, 2021; accepted May 19, 2021. Date of publication May 24, 2021; date of current version October 27, 2021. *(John W. Hayes and Juan Montoya are co-first authors.) (Corresponding author: Guang-Hong Chen.)*

This work involved human subjects or animals in its research. Approval of all ethical and experimental procedures and protocols was granted by the University of Wisconsin-Madison.

John W. Hayes, Juan Montoya, Chengzhu Zhang, Yinsheng Li, Ke Li, and Guang-Hong Chen are with the Department of Medical Physics, School of Medicine and Public Health, University of Wisconsin-Madison, Madison, WI 53705 USA (e-mail: gchen7@wisc.edu).

Adam Budde and Jiang Hsieh are with GE Healthcare, Chicago, IL 60642 USA, and also with the Department of Medical Physics, School of Medicine and Public Health, University of Wisconsin-Madison, Madison, WI 53705 USA.

Digital Object Identifier 10.1109/TMI.2021.3083210

dose to the patient is inversely proportional to the normalized helical pitch p, high helical pitch scans are preferred for radiation dose reduction purposes; 2) High helical pitch scanning improves image quality in cardiac CT scans [12]. To complete a cardiac CT exam with 4.0 cm z-coverage in current 64-slice CT scans, the cardiac CT image volume of the entire heart consists of image slabs from four different heart beats. Due to the potential inconsistency from one heart beat to another, the uniformity in image quality across the four slabs is limited. With high helical pitch scans, the quality of uniformity can be significantly improved; 3) High helical pitch CT scans increase the scan throughput to improve the workflow in current healthcare systems; 4) With high pitch scans, the same scan volume coverage and other benefits offered by high-end CT scanners, e.g., 256-slice MDCT scanners, can be achieved with lower-end scanners such as 64-slice MDCT scanners. This can reduce the total manufacturing costs of scanners due to the fact that there are almost no mechanical challenges nor safety concerns for patients to increase table translation speed by a factor of 2-4 for the current speeds used in most single source MDCT scanners.

Therefore, to enable low cost, low dose, and high quality CT scans, it is critically important to address the scientific challenges in high pitch $p \geq 1.5$ helical CT reconstruction problems. This is the focus of our work in this paper. Specifically, to address the view angle undersampling problem and limited view problem in high pitch helical CT reconstruction problems, we show that the synergistic use of the following three techniques can be used to enable accurate helical CT reconstruction for pitch up to 4.0: 1) A data interpolation scheme was introduced to approximately fill the missing view angles in high pitch helical scans and then a conventional 3D Fledkamp reconstruction algorithm (FDK) is used to reconstruct the initial images. 2) A deep learning scheme was introduced to transform the initially reconstructed image with residual artifacts into high quality images. 3) If the quality of the deep learning output is not satisfactory, the deep learning output image is used as the prior image in prior image constrained compressed sensing (PICCS) [13] to further improve quality. While the data interpolation for helical FBP in step 1 is similar to other well known techniques, steps 2 and 3 represent major innovations introduced in this work. As it is shown in the results, depending upon the number of detector rows used in MDCT scanners, the above strategies in image reconstruction enables accurate helical CT reconstruction for pitch up to $p = 4$ for 16-, 32-, and 64-slice CT scanners.

II. Methods

A. Challenges in View Angle Sampling Range for High Pitch Helical Acquisition

To achieve accurate CT reconstruction, two conditions must be satisfied: 1) the view angle range must satisfy the so-called Tuy data sufficiency condition [11] to avoid limited view shading artifacts and 2) the view angle sampling density must be dense enough to avoid aliasing artifacts which are often present in reconstructed images as streaky artifacts.

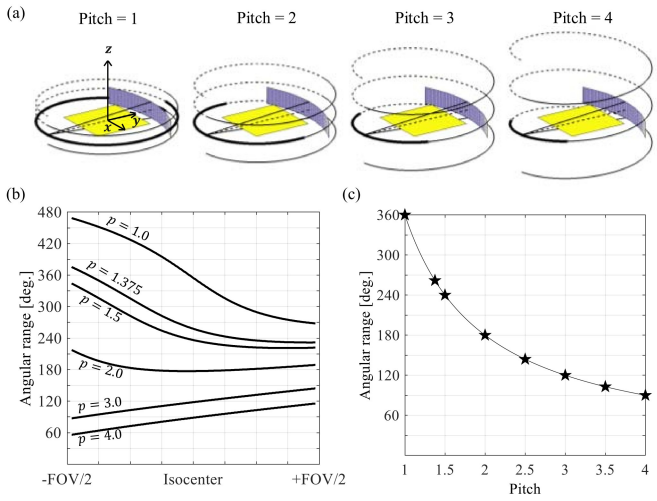

Fig. 1. (a) Helical trajectories with three revolutions around a given reconstruction plane (shown in yellow) for each pitch. The illuminating range for this plane is shown in solid black. (b) Illuminating range of image pixels along the line crossing the isocenter is plotted for different helical pitches. (c) The star marks the illuminating range for the isocenter as a function of pitch.

These conditions are used to ensure that there are sufficient x-ray illuminations for each image voxel for the voxel to be accurately reconstructed.

When helical CT is considered, the illumination of an image voxel in a given reconstruction plane at $z = z_0$ is a function of the helical pitch p. When p is increased, the angular range of the x-ray illumination decreases. As shown in Fig. 1(a) for $p = 1$, 2, 3, and 4, higher helical pitches result in smaller angular illumination ranges of the voxel at isocenter on the given reconstruction plane. Note that different image voxels in the reconstruction plane may have different illuminating ranges, but these also decrease with increasing pitch. This is shown for the voxels along the lines passing through the isocenter as shown in Fig. 1(b) for 6 different pitches from $p = 1$ to $p = 4$. To highlight the decrease of illuminating range, the change of illuminating range with helical pitch is presented in Fig. 1(c). As one can see, the illuminating range for the voxel at isocenter can go from fully illuminated at all view angles at $p = 1$ down to about 90° for an MDCT scanner with fan angle of $\gamma_m \approx 60°$.

For helical trajectories, Fig. 1(b-c) shows sampling in the plane remains at or above the short scan range for pitch $p \lesssim 1.375$ to satisfy the Tuy data sufficiency condition, but falls below this threshold for higher pitches. As a result, analytical reconstruction methods that in theory require sampling to at least meet the short scan condition will yield limited view artifacts in images reconstructed for pitch $p > 1.375$. Note that, in practice, some sorts of data extrapolation schemes have also been introduced by CT vendors to extend the helical pitch up to $p \lesssim 1.5$.

B. Data Augmentation to Extend the Illuminating Window and FBP Reconstruction

The first step in our proposed high pitch helical reconstruction scheme is to reconstruct an initial image $\mathbf{x_F}$ directly from

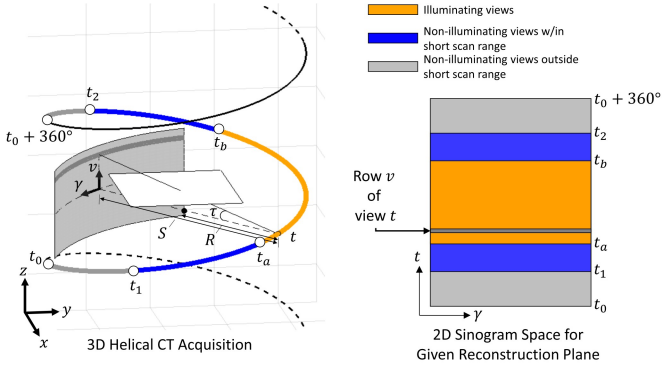

Fig. 2. Illustration of the 3D FDK algorithm for helical scans. (a) The source-detector system during helical acquisition is shown relative to a given axial reconstruction plane. The range of views $[t_a, t_b]$ illuminating isocenter on the plane is colored with a thick orange line. Views outside the detector FOV for this plane are colored with a thick blue line (within the short scan range) or a thick gray line (outside the short scan range). (b) The data filling scheme for the 2D sinogram to reconstruct the given axial plane. The detector row v where isocenter projects onto the detector is filled in 2D sinogram space according to the steps outlined.

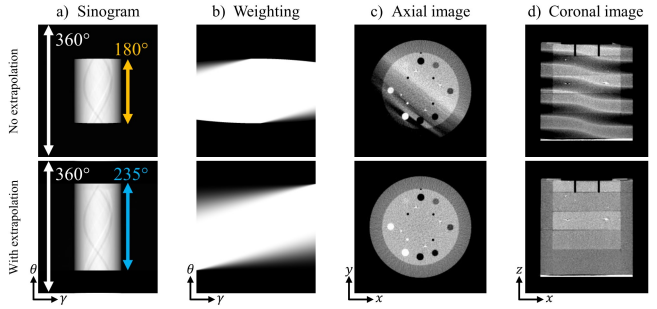

Fig. 3. 3D FDK reconstructions both with and without extrapolation of the Catphan phantom for an experimental helical scan with pitch 2. The 2D projected sinogram (a) is given Parker weights (b) and reconstructed to the axial slice shown (c). The coronal image (d) is reformatted from the reconstruction of 2D projected sinograms for all axial slices.

the CT scan raw data using FBP. The specific algorithm in this work is the 3D FDK [14] algorithm adapted for helical trajectories. However, severe artifacts will be introduced due to the illustrated high helical pitch reconstruction problem in the previous section. In this work, data augmentation techniques were introduced to first extend the illumination range of all image voxels in the reconstruction plane to short scan illuminating range. Then, a 3D FDK reconstruction, which converts a 3D cone beam reconstruction problem into a series of 2D fan beam reconstruction problems, is performed to reconstruct the initial image $\mathbf{x_F}$.

The steps to form the FBP image volume are given below and are illustrated graphically in Fig. 2:

1) For a given reconstruction plane, find the range of views $[t_a, t_b]$ that illuminate isocenter on that plane.
2) For each view $t \in [t_a, t_b]$, find the detector row v where isocenter projects onto the detector plane.
3) Weight the data in row v by $\cos\tau$, where $\tau = \arctan(v/S)$ and use the result to fill a single row of 2D sinogram space at view t.
4) For each view $t \in [t_1, t_a]$ and $t \in [t_b, t_2]$ that does not illuminate isocenter on the plane, use the top and bottom row respectively for Step 3. Here, $[t_1, t_2]$ defines a short scan angular range of $180° + \gamma_m$.
5) For each view $t \in [t_0, t_1]$ and $t \in [t_2, t_0 + 360°]$ that does not illuminate isocenter on the plane, use a zero row for Step 3. These ranges are outside the short scan angular range centered on the plane.
6) Apply Parker weighting in the range $[t_1, t_2]$ for the 2D sinogram
7) Perform 2D fan-beam FBP reconstruction of the sinogram formed for this plane.
8) Repeat Steps 1-7 for every axial reconstruction plane in the image volume.

To demonstrate the need for data extrapolation (step 4 above) in helical FBP, CT data was acquired for a Catphan phantom (Catphan 600, Phantom Laboratory, Salem, New York) on a 64 slice MDCT scanner (GE Discovery CT750 HD, Waukesha, WI). The data was numerically collimated to yield a scan with helical pitch 2 and was reconstructed both with and without data extrapolation. Results are shown in Fig. 3. The phantom images have severe shading artifacts using the FBP reconstruction without data extrapolation due to the limited angular range. The limited view shading artifacts have been removed however in FBP with data extrapolation.

C. Deep Learning to Correct FBP Reconstructed Images

Without further correction, the FBP reconstructed images with data interpolations cannot be accurate. To correct these FBP reconstructed images, a deep learning strategy was introduced. We present the neural network architecture and our training strategies in the following subsections.

1) Neural Network Architecture: The neural network was designed to correct 2D image slices within the 3D volumes. We used a multi-stage modular design where multiple U-Nets [15] were stacked together in order to reduce the helical artifacts along the 2D axial image planes followed by correction along the 2D coronal image planes. Each U-Net consisted of 24 convolutional layers arranged in 4 vertical levels. The network architecture is shown in Fig. 4.

The aforementioned stacked U-Net architectures were trained for each given helical pitch values $p = 2, 3, 4$ and for each detector configuration $N_v = 16, 32, 64$ for 16-, 32-, and 64-slice MDCT. As a result, a total of 9 separate artifact removal networks were individually trained.

The output of the network had $288 \times 288 \times N_z$ voxels with the same resolution as the input with 545 mm in-plane field of view (FOV) and 1 mm slice thickness ($1.89\,\text{mm} \times 1.89\,\text{mm} \times 1.00\,\text{mm}$).

2) Training Strategy: The network was trained using a conditional adversarial strategy [16], [17] where an adversarial loss aims to minimize the L1-loss between input artifact contaminated FBP images and the target clinical CT images while maximizing an image discriminator cross-entropy loss between the network output and clinical CT images to assure that the artifact corrected images follow the same distribution